Insight into the atomic structure of cycled lithium-rich layered oxide Li1.20Mn0.54Co0.13Ni0.13O2 using HAADF STEM and electron Nanodiffraction

Cécile Genevois, Hideyuki Koga, Laurence Croguennec, Michel Ménétrier, Claude Delmas, François Weill

THE JOURNAL OF PHYSICAL CHEMISTRY C

Article

Insight in the Atomic Structure of Cycled Lithium-rich Layered Oxide Li1.20Mn0.54Co0.13Ni0.13O2 using HAADF STEM and Electron Nano Diffraction

Cecile Genevois, Hideyuki Koga, Laurence Croguennec, Michel Ménétrier, Claude Delmas, and François Weill

J. Phys. Chem. C, **Just Accepted Manuscript** • Publication Date (Web): 10 Dec 2014

Genevois et al. - 09/12/2014 submitted to J. Phys. Chem. C

Insight in the Atomic Structure of Cycled Lithium-rich Layered Oxide $Li_{1.20}Mn_{0.54}Co_{0.13}Ni_{0.13}O_2$ using HAADF STEM and Electron Nano Diffraction

Cécile Genevois [1,§], Hideyuki Koga [2,3], Laurence Croguennec [2,*], Michel Ménétrier [2], Claude Delmas [2] and François Weill [2,*]

[1] *Groupe de Physique des Matériaux, Université et INSA de Rouen, UMR6634 CNRS, avenue de l'Université, BP12, F-76801 Saint Etienne du Rouvray, France*

[2] *CNRS, Univ. Bordeaux, ICMCB UPR9048 and IPB-ENSCBP, F-33600 Pessac, France*

[3] *TOYOTA MOTOR EUROPE NV/SA - Hoge Wei 33, B-1930 Zaventem, Belgium*

KEYWORDS

Lithium batteries; Positive electrode; Layered oxide; Overcapacity; Transmission electron microscopy; Twins; Cation ordering; Cation migration;

ABSTRACT

Aberration-corrected high-angle annular dark-field scanning transmission electron microscopy (HAADF STEM) and electron nano diffraction investigations have been carried out to follow changes in the local atomic structure of three Li-rich layered oxides recovered after a single charge-discharge cycle, performed in different conditions. The structure of the pristine material $Li_{1.20}Mn_{0.54}Co_{0.13}Ni_{0.13}O_2$ was fully characterized. It was then compared to those of the materials recovered after one electrochemical cycle in a lithium battery, with the upper voltage limit being either just below the voltage of the irreversible "plateau" typical of Li-rich layered oxides, or just above. An in-depth study of the material obtained chemically, after an oxidation to deintercalate Li and then a reduction to reintercalate Li, was also performed for comparison. The main message of this paper is that the "plateau" is not associated to an extended structural reorganization of the material. The irreversible processes associated to cation migration are restricted to the external part of the particles. The results reported here support the oxidation of oxygen ions we have earlier proposed to occur reversibly in the core of the particles and to be the actual origin for the exceptional capacity of Li and Mn-rich layered oxides.

* Corresponding authors: ☎ +33 (0) 5 4000 2234; ✉ crog@icmcb-bordeaux.cnrs.fr (L. Croguennec) - ☎ +33 (0) 5 4000 2654; ✉ weill@icmcb-bordeaux.cnrs.fr (F. Weill)

§ Present address: CNRS, CEMHTI UPR3079, Univ. Orléans, F-45071 Orléans, France

I. INTRODUCTION

The Li- and Mn-rich layered oxides (that can also be written as (1-y)Li_2MnO_3.y$LiMO_2$ (M = Mn, Co, Ni) according to the notation proposed by M.M. Thackeray, with the overall Li/M ratio higher than 1) currently attract considerable attention as most promising positive electrode materials due to their very high energy density[1-5]. Some authors consider that they are composed of two phases (or domains), namely Li_2MnO_3 and ideal layered $LiMO_2$[6-9], while others propose that a "solid solution" (i.e. a homogeneous cation distribution) exists with a cation ordering in the transition metal layers[10-15]. The recent results reported by McCalla et al. have clearly demonstrated that, depending on the composition, the oxygen partial pressure and the cooling rate can be critical to control the formation of a single phase, essential to deliver good electrochemical performances[16-19]. It is well known that in Li_2MnO_3 (*i.e.* $Li(Li_{1/3}Mn_{2/3})O_2$, described in the space group *C2/m*) the difference in size between the Li^+ and Mn^{4+} ions with a Li/Mn ratio of 1/2 leads to a complete ordering within the transition metal layers **(Figure 1** and **Table S1**, see supporting information for that latter**)**[20-21]. In ideal 2D $LiMO_2$ layered oxides (described in the space group *R-3m*), extended ordering can be observed within the slabs only for the $Li(Ni_{1/3}Mn_{1/3}Co_{1/3})O_2$ composition that exhibits the ideal 1/2 ratio between the large (Ni^{2+}) and the small (Mn^{4+} and Co^{3+}) cations. In the case of the Li-rich layered oxides, only those belonging to the (1-X)Li_2MnO_3.X$Li(Ni_{1/3}Mn_{1/3}Co_{1/3})O_2$ system thus exhibit the ideal composition required to establish an extended cation ordering within the slabs; nevertheless, a tendency to ordering with a symmetry change can be observed for compositions slightly different from ideal ones[22]. These considerations can explain discrepancies in literature reports.

The aim of this paper is to get more insight in the atomic structure of the $Li_{1.20}Mn_{0.54}Co_{0.13}Ni_{0.13}O_2$ material revealed to be very attractive as positive electrode for lithium-ion batteries, using very powerful techniques such as electron nano-diffraction and aberration-corrected high-angle annular dark-field scanning transmission electron microscopy (HAADF-STEM) imaging with a probe size of 0.1 nm. The material was shown to be homogeneous at all length scales with an ordering among two crystallographic sites of the large cations (Li^+, Ni^{2+}) on one side (~0.70 Å) and the small cations (Mn^{4+}, Co^{3+}) on the other side (~0.54 Å) (**Table S1**). The nature of the cations was determined combining especially X-ray and neutron diffraction, both being complementary[15]. We clearly evidenced by electron diffraction the ordering in the transition metal layers, with the absence of an extended long range ordering perpendicularly to them. This cation distribution is in very good agreement with the expectations, as a way to minimize the strains in this structure that contains four cations (Li^+, Ni^{2+}, Mn^{4+} and Co^{3+}) in the slabs. With nano-diffraction, the homogeneity of the atomic structure can be checked within and among the crystals (from the surface to the bulk). As HAADF-STEM discriminates atoms with small and large Z electron numbers[23], it allows determining the extent of the cation ordering within the transition metal layers and the nature of the stacking between the ordered slabs along the c-axis. Getting this in-depth understanding of the atomic structure of $Li_{1.20}Mn_{0.54}Co_{0.13}Ni_{0.13}O_2$ is essential to study the structural modifications occurring upon cycling and to establish a link with the peculiar mechanism involved in these positive electrode materials. Indeed, we recently proposed that oxidation

of oxygen from the outer part of the particles leads to oxygen loss and reconstruction of this part of the material during the first charge, whereas oxygen in the bulk of the material reversibly participates in the redox process without major modification of the structure[24-26]. Note that recently Sathiya et al. came also to that conclusion, *i.e.* the reversible participation of oxygen to the redox properties, for the $Li_2Ru_{1-y}Sn_yO_2$ system, a Li-rich layered oxide that shows also an irreversible high voltage plateau during the first charge and an overcapacity versus the number of electrons that can be exchanged considering the transition metal ions only[27].

II. EXPERIMENTAL

$Li_{1.20}Mn_{0.54}Co_{0.13}Ni_{0.13}O_2$ was obtained by a sol-gel method from an aqueous solution of $Li(CH_3COO)$ (99 % Aldrich), $Mn(CH_3COO)_2.4H_2O$ (99 % Aldrich), $Co(CH_3COO)_2.4H_2O$ (99 % Fluka), $Ni(CH_3COO)_2.4H_2O$ (99 % Aldrich) and Glycolic acid (99 % Fluka) as chelating agent. A detailed description of the preparation of the material as well as its full characterization is reported in ref 15. Using chemical and redox titrations, diffraction (X-rays, neutrons and electrons), magnetic measurements as well as NMR and Raman spectroscopy, the material was shown to be characterized by the formula $[Li_{0.98}Ni^{II}_{0.02}]_{Interslab\ space}[Li_{0.22}Ni^{II}_{0.11}Mn^{IV}_{0.54}Co^{III}_{0.13}]_{Slabs}O_2$ and to be homogeneous at all length scales[15].

The positive electrodes consisted of 80 wt% of active material, 10 wt% of a carbon black / graphite (1:1) mixture and 10 wt% of polyvinylidene fluoride (PVdF) binder cast on an aluminum foil. They were then pressed at 40 MPa after being dried at 80°C during overnight. Coin cells were assembled in an argon filled glove box with Li metal as counter electrode and 1M $LiPF_6$ dissolved in a mixture of propylene carbonate (PC), ethylene carbonate (EC), and dimethylcarbonate (DMC) 1:1:3 by volume, as electrolyte. A first sample was recovered from the battery after a charge before the “plateau” and a discharge. Another sample was also recovered from the battery, but after a 1st charge up to 4.8 V vs. Li^+/Li (i.e. after the “plateau”) and a discharge, as shown in **figure 2**.

Li was also deintercalated chemically from $Li_{1.20}Mn_{0.54}Co_{0.13}Ni_{0.13}O_2$, which was preliminarily dried at 120°C overnight, by dropping a 0.3M NO_2BF_4 acetonitrile solution into a suspension of the $Li_{1.20}Mn_{0.54}Co_{0.13}Ni_{0.13}O_2$ powder in acetonitrile. The mixture obtained was maintained under stirring for 1 day. Chemical Li reinsertion was performed by adding an 0.3M LiI acetonitrile solution to the material previously chemically deintercalated in suspension in acetonitrile, stirring was maintained for 3 days. The powder obtained after chemical Li deintercalation and reinsertion was washed thoroughly with acetonitrile. These chemical Li deintercalation and reinsertion were carried out in an argon filled glove box. As reported by some of us in ref 25, the material obtained after chemical Li deintercalation and reintercalation was fully characterized. It was shown to be very similar in composition, structure and electrochemical properties to that obtained electrochemically after one cycle from batteries.

Prior to the observation in transmission electron microscopy, a suspension was obtained by grinding the material in hexane, a droplet of this suspension being deposited on a formvar carbon film supported on a copper grid. Electron diffraction experiments were carried out on many crystallites and

very reproducible results were observed. The particles studied were chosen as isolated as possible. HAADF-STEM images and electron nanodiffraction patterns were obtained using a JEM ARM200F microscope. HAADF-STEM images were performed in different domains of the particles, thin enough, due to limitations in resolution by thickness. To simplify the comparisons we use the *R-3m* space group described in its hexagonal setting, to discuss the electron diffraction results and the structural properties.

III. RESULTS AND DISCUSSION

1. The pristine material

Prior to any characterization of materials recovered after cycling, an in-depth knowledge of the pristine material was required to ascertain the homogeneity between particles and within each particle, from the surface to the bulk. This first step is compulsory to use this material as a reference, since it is known that any small change in synthesis conditions and in the composition can be at the origin of significant differences in the atomic distribution at the local scale within the Lithium and Manganese-rich materials.

To characterize the transition metal ordering in the transition metal layers, it is necessary, in the transmission electron microscope, to view the material along one of the three equivalent directions $[-110]_{R\text{-}3m}$, $[210]_{R\text{-}3m}$ and $[120]_{R\text{-}3m}$ indicated in **figure 1** by the red, blue and green arrows respectively. Indeed, along these directions, the atomic columns only contain atoms belonging to one type of crystallographic site (Mn or Li in the case of Li_2MnO_3). **Figure 3** presents a typical HAADF-STEM image of the material viewed along one of these directions.

On the image given in **figure 3**, the lamellar character of the structure is clearly visible with lines of bright dots separated with lines of only dark dots. As a matter of fact, the contrast in this type of images is in first approximation proportional to $Z^{1.7}$. Thus, in our material, only the transition metal atoms appear as white dots, whereas lithium and oxygen atoms are not visible since they correspond to dark dots. As expected, the slab with mainly transition metal atoms appears with bright dots (orange arrow) whereas the interslab space, with mainly lithium atoms, is not observed (orange and white arrow). In the slab, an ordering between the cations is also clearly observed with the contrast of the image (two bright dots - one darker dot) corresponding to the order Heavy-Heavy-Light. Considering that $H_{(Heavy)}$ = (20% Co^{3+}, 80% Mn^{4+}) and $L_{(light)}$ = (60% Li^{+}, 40% Ni^{2+}), this fully corresponds to the expected ordering based on size considerations and, as already discussed above, in agreement with XRD an neutron diffraction data [15]. It is also interesting to look carefully at the stacking of the transition metal layers. Obviously three different stackings, materialized by colored lines in **figure 3** can be observed and the extent of the corresponding domains is up to six or seven slabs. The stacking pointed out by the red, blue and green lines in **figure 3** correspond exactly to the ideal stacking of the ordered transition metal layers observed in various directions of the Li_2MnO_3 model compound. Indeed,

the experimental image can be directly compared to the projections of the structure of Li_2MnO_3 along the $[-110]_{R\text{-}3m}$, $[210]_{R\text{-}3m}$ and $[120]_{R\text{-}3m}$ directions given in **figure 4**. These directions are perpendicular to the $c_{hex.}$ axis and separated from each other by 60°. The crystallites, and it is a general observation for this material, are then twinned. In this ideal stacking of Li_2MnO_3, the actual crystalline symmetry is lowered to monoclinic (space group *C2/m*). In the electron diffraction pattern corresponding to each projection, the additional reflections corresponding to this lowering of symmetry are underlined by red arrows.

In good agreement with these observations, the electron diffraction pattern given in **figure 5a** shows three rows of intense reflections that can be indexed in the *R-3m* space group used to describe the structure of the ideal O3-type layered materials. Diffuse lines parallel to c* are also visible between the rows of the main reflections; they divide the [110] distance by three and are the signature of a two-dimensional ordering in the transition metal layers[21]. Nevertheless, the intensity along the diffuse lines is not homogeneous since spots corresponding to the lowering of the symmetry (highlighted by red arrows in **figure 4c)** can be obviously distinguished.

Note that if one considers only the main reflections of the electron diffraction pattern corresponding to the non-ordered R-3m structure, the three theoretical electron diffraction patterns can be exactly superimposed since the rotation between them is 60°. Only the location of the additional reflections can discriminate between the projections. These observations and their interpretation were already done and proposed by Boulineau *et al.* on a rather different composition ($Li_{1.20}Mn_{0.61}Ni_{0.18}Mg_{0.01}O_2$)[28]. The inset given in **figure 3** shows the theoretical image calculated considering the alternating stacking of two types of domains along the c_{hex} axis. Obviously the theoretical image is very similar to the experimental one. Note that the calculation was performed considering a hypothetical Li_2MnO_3 composition with the cell parameters of our compound $Li_{1.20}Mn_{0.54}Co_{0.13}Ni_{0.13}O_2$. The corresponding electron diffraction pattern is also compared to the experimental one in **figure 5**. The additional reflections observed in the experimental diffraction pattern are less defined than the corresponding ones in the theoretical pattern (**Figure 5**), in good agreement with an actual stacking of the twin components less ordered than that used to calculate the theoretical pattern.

To check for the homogeneity of the crystallites, nano-diffraction experiments were performed. **Figure 6** presents a set of typical nano-diffraction patterns obtained in a single crystal at different locations, as shown in **figure 6a** each probed area being 45 nm in diameter. Even if the probe size is rather large compared to the size of the twin components, the nano-diffraction patterns can give a general trend. The information obtained using this technique is intermediate between that obtained from selected area diffraction patterns and from images. The pattern in **figure 6b** originates from area ⑥ and corresponds to the blue stacking of **figure 4b**, while the pattern in **figure 6c** is typical of areas ①, ②, ③ and ⑦. In these areas, the predominant twin components correspond to the red and green stackings of **figures 4a and 4c**. The pattern in **figure 6d** is typical of areas ④, ⑤, ⑧ and ⑨, none of the twin components are predominant. No additional reflection could be observed in any part of the

crystallite studied. The same type of observations was made on all the crystallites explored by this technique. Note that area ⑥ corresponds to an ideal stacking of ordered slabs along one single direction, i.e. [210], and that it is mainly surrounded by domains showing nano-twins, i.e. changes in the orientation of the ordered slabs within a short distance (areas ④, ⑤, ⑧ and ⑨).

Note that very locally, as for instance in the slab indicated by a red arrow on **figure 3**, a more uniform contrast is observed. Such slabs with an almost uniform contrast have also been observed previously, and they have been interpreted as the evidence of the occurrence of a second non ordered phase (or domains) corresponding to an ideal layered $LiMO_2$-type phase in one crystallite[28]. Their occurrence was analyzed to be in accordance with the description 0.6 $Li[Li_{1/3}Mn_{2/3}]O_2$. 0.4 $LiNi_{0.45}Mn_{0.525}Mg_{0.025}O_2$ of the material $Li_{1.2}Mn_{0.61}Ni_{0.18}Mg_{0.01}O_2$. Nevertheless, in our case, the frequency of appearance of such apparently non-ordered slabs is rather low. They do not appear in all the crystallites and the thickness of these non-ordered domains is limited to one or two slabs. The relative amount of these disordered slabs versus the ordered ones is obviously very different from what one could have expected (i.e. 50%) if the material was made of separated domains of Li_2MnO_3 on the one hand and of $LiNi_{1/3}Mn_{1/3}Co_{1/3}O_2$ on the other hand. Note that the difference in local structure observed between $Li_{1.20}Mn_{0.54}Co_{0.13}Ni_{0.13}O_2$ and $Li_{1.2}Mn_{0.61}Ni_{0.18}Mg_{0.01}O_2$ is in fact expected. Indeed, the former is characterized by a ratio (number of large cations)/(number of small cations) within the slabs of 1/2, as in the ordered structure of Li_2MnO_3, whereas the latter is characterized by a ratio close to 1/1 that prevents, “by definition”, any extended ordering within the slabs. We therefore propose another interpretation to the observation of these non-ordered slabs. As illustrated on **figure 7**, the domain wall can be localized within a transition metal layer, forming a stair step between the two adjacent domains. The frontier between the two domains can thus be perpendicular to the direction of observation of the columns of atoms. As the images observed by STEM or TEM are bidimensional projections in the whole thickness of a crystal, the transition metal layer where this happens will therefore appear as disordered. For the $Li_{1.20}Mn_{0.54}Co_{0.13}Ni_{0.13}O_2$ composition, the Li_2MnO_3 type ordering is locally observed with various orientations leading to domain formations in all parts of the crystallites. In some places, one transition metal layer appears to be ordered and then disordered. This may happen if the wall between two adjacent domains goes through the transition metal layer, but in a direction perpendicular to the observation one. All this is possible because the oxygen network is the same in the whole crystallite and the domain only results from the ordering of the cations in the transition metal layers. The presence of micro-domains thus explains, by itself, all the observations made on the images (**Figure 3**) as well as on the diffraction patterns (**Figure 6**). Area ⑥ of **figure 6a** corresponds to a single type domain, and is surrounded by areas ④, ⑤, ⑧ and ⑨ that contain several domains and stair steps as that described in **figure 7**.

2. The materials obtained upon Lithium deintercalation and reintercalation

Characterization of cycled materials is not straightforward, especially in their oxidized state (in the charged state of the battery) at which most of them are unstable: during their observation in TEM, the

electron beam produces irreversible damages and the actual structural modifications induced by the electrochemical processes is no longer be observable. As the goal of this study is to determine if an extended structural reorganization with cation migration occurs during the first charge of $Li_{1.20}Mn_{0.54}Co_{0.13}Ni_{0.13}O_2$, we chose to compare the pristine material to different materials recovered after one cycle (*i.e.* with a lithium content close to 1): in that case the results obtained are representative of the mechanisms involved during lithium deintercalation and reintercalation because the materials were shown to be stable under the electron beam.

Representative HAADF-STEM images of the material recovered after the 1st cycle without the "plateau" are given in **figures 8a and 8b**. These images could be obtained in thin parts of the particle studied and are very similar to that shown in **figure 3** for the pristine material. The ordering observed in the transition metal layers (H-H-L) is not affected, as well as the extent of the 2D lamellar character. No obvious presence of transition metal ions is observed in the Li sites. **Figures 8c and 8d** show for comparison images representative of the material recovered after the 1st cycle of the battery including the "plateau". The ordering (H-H-L) in the transition metal layers is still largely maintained as shown in **figure 8c**, nevertheless some dark dots from the sequence bright dot - bright dot - dark dot are clearly less visible (they are whitened). In addition, bright dots appear also in some Li layers as indicated by arrows in **figure 8d**. This suggests, first, that upon cycling at high voltage on the "plateau" transition metal ions have migrated to vacancies formed in the slabs by Li deintercalation and, then, that some others have also migrated from the slabs to the interslabs[29]. These images are in rather good agreement with (at least) a partial densification of the host structure of the material. These observations show clearly, as expected from our previous results obtained by X-ray diffraction mainly[24-25], that the migration of transition metal ions is observed only when the battery is charged at higher voltage after the "plateau". The main point here to highlight is that the densified/reorganized domains are not dominant (extended) after one cycle. These observations fully support the mechanism we proposed to explain the lithium deintercalation and reintercalation reaction in these materials: the densification process, which results from the oxygen loss from the structure, is restricted to the outer part of the particles and is far from being able to compensate by itself for all the lithium ions deintercalated on the "plateau"[24-26].

In order to fully support these results, we chose to study in parallel the material prepared chemically by Li deintercalation using NO_2BF_4 and Li reintercalation with LiI. As previously reported in[25], materials prepared by chemical Li deintercalation with NO_2BF_4 from $Li_{1.20}Mn_{0.54}Co_{0.13}Ni_{0.13}O_2$ and chemical Li reinsertion with LiI show very similar chemical composition, oxidation state of each transition metal ion, structural properties and electrochemical performance to those of the material recovered after the 1st electrochemical cycle (see Figure 5 in ref 25). That material prepared chemically was largely analyzed using HAADF-STEM and nano-diffraction to study the detailed structural changes of $Li_{1.20}Mn_{0.54}Co_{0.13}Ni_{0.13}O_2$ during the 1st cycle. **Figure 9** shows representative HAADF STEM images of the crystallites observed for the material prepared chemically. The ordering (H-H-L) in the transition metal layers is maintained in the internal parts of the crystals, within the bulk as shown in **figure 9a**, but in external parts some transition metals have migrated into the vacancies formed by Li deintercalation

from the slabs but also from the slabs to the interslab spaces in the sites previously occupied by Li^+ ions, more at the surface as shown in **figure 9b**. The transition metals having migrated in the interslabs appear to be rather ordered as shown in **figure 9b** (sequence bright dot - black dot). These analyses further confirm that densification, at least partial, occurs in some parts of the crystals whereas the pristine structure is maintained in other parts. This results support again the heterogeneous reaction occurring during the 1st cycle with the formation of "two" phases as reported in the ref 24.

Analysis using nano-diffraction was also performed in order to screen the particles from the surface to the bulk, as shown in **figure 10**, and to confirm the difference in structures between the surface and the bulk. For patterns 1 and 2, the additional spots present between the diffusion lines reveal the formation of defects near the surface[20]. On the contrary, their absence shows that the initial structure is maintained within the bulk. These results reveal again the formation of heterogeneous particles during the 1st cycle. These observations are in good agreement with the results just discussed above and with other analyses performed in our group[24-26].

Concerning the nature of the defects, to discuss further the (H-L) ordering (sequence of bright dot - black dot) observed in the interslab space in **figure 9b**, it is interesting to consider the inset that compares the experimental image to the one expected for an ideal spinel structure LiM_2O_4, that can be also described as a layered structure with transition metals in the interslab space $[Li_{0.5,Td}M_{0.25,Oh}][M_{0.75}\square_{0.25}]_{Oh}O_2$ (Td and Oh: in tetrahedral and octahedral sites respectively). Indeed, the continuous potential decrease observed for these Li-rich layered oxides upon cycling is often assumed to be associated to transformation of the layered structure to the spinel one. Note that the (H-L) ordering observed in the interslab is that expected for a spinel structure. Nevertheless, from the simulated image of LiM_2O_4 a sequence "strongly" bright dot - "weakly" bright dot is expected for the slabs. This sequence is actually not observed in the experimental image. Two main sequences are in fact observed: (i) a rather homogenous intensity within the transition metal atomic layer or (ii) "strongly" bright dot - "strongly" bright dot - "weakly" bright dot. As already discussed, images correspond to bidimensional projections in the whole thickness of the crystal: it thus strongly suggests that the atomic columns observed in **figure 9b** are in fact the "sum" of domains with defects (more on the external part) and layered-type domains (dense or not). The domains with defects formed are characterized by a $c_{hex.}/a_{hex.}$ ratio of 5.0 (vs. 4.90 expected for an ideal ordered spinel)[24], still typical of a layered structure, and by the presence of transition metal ions in octahedral sites in the interslabs. The structure of these domains with defects could be perhaps also referred to as "splayered"[30], i.e. between layered and spinel. Indeed, the octahedral sites of the interslabs are partially occupied as in a spinel structure, whereas the slabs keep memory of the Li_2MnO_3-type order observed in the pristine material.

If we compare our results obtained using STEM-HAADF to those recently reported by Boulineau *et al.*[28, 31] for the Li-rich composition $Li_{1.2}Mn_{0.61}Ni_{0.18}Mg_{0.01}O_2$, it is interesting to highlight that after the first cycle at high voltage the observations are similar. Indeed, there is heterogeneity within the particles with a structure with defects at the surface and a layered structure maintained within the bulk. Nevertheless, in our case whatever the conditions used to prepare the material (electrochemical or chemical), the

extent of the domains with defects is more restricted. Two reasons can be considered to rationalize this observation: (i) The $Li_{1.2}Mn_{0.61}Ni_{0.18}Mg_{0.01}O_2$ material is a composite with only a partial "solid solution" and the formation of Li_2MnO_3 and $LiNi_{0.45}Mn_{0.525}Mg_{0.025}O_2$ domains, contrary to our $Li_{1.20}Mn_{0.54}Co_{0.13}Ni_{0.13}O_2$ material that shows an extended "solid solution"; (ii) a peculiarity of the $Li_{1.2}Mn_{0.61}Ni_{0.18}Mg_{0.01}O_2$ material is also that it contains about 25% of Mn^{3+} among the total amount of Mn and this could be the actual origin of this extended formation of domains with defects. Indeed, for Mn^{3+}-rich $LiMnO_2$ layered oxides, a systematic transformation of the layered to a splayered structure is observed upon cycling through migration of manganese from the slab to the interslab[32-33]. Boulineau et al. have also shown that, for the composition they studied, after 50 cycles the size of the domain with defects remains limited. Nevertheless, the densification extends continuously upon cycling with the preferential migration of manganese cations from the surface to the bulk leading thus to an increasing nickel concentration at the surface[31]. As mentioned above, Sathiya et al. studied different $Li_2Ru_{1-y}M_yO_2$ layered oxides materials (M = Sn, Ti, Mn)[27, 34-35], in order to determine also the cause of the voltage decay observed upon cycling and leading to a continuous decrease of the energy delivered by these lithium-rich materials despite their large reversible capacity. They have shown that the voltage decay is maximum for Ti-substituted materials and minimum for Sn-substituted ones, and in addition using also STEM-HAADF that this trend follows the extent of cationic reorganization[35]. The more extended the cationic reorganization is, the larger is the domain with defects formed and the larger is the voltage decay.

IV. CONCLUSIONS

The nanostructure of the $Li_{1.20}Mn_{0.54}Co_{0.13}Ni_{0.13}O_2$ material has been explored using nano-diffraction experiments and STEM-HAADF images, for the pristine composition and for materials recovered from the batteries after the 1st cycle, with and without the "plateau", and for the material prepared by a chemical Li reinsertion after a chemical Li deintercalation. First, our study further evidences that the $Li_{1.20}Mn_{0.54}Co_{0.13}Ni_{0.13}O_2$ composition we have studied is a "solid solution" with ordered transition metal layers and not a composite made of Li_2MnO_3 and $LiNi_{1/3}Mn_{1/3}Co_{1/3}O_2$ domains. The stacking of these ordered layers gives rise to twins in all the crystallites, with an average domain size around six to seven slabs. The goal here was to support further the mechanism we proposed to explain the exceptional capacity of these Li-rich materials, *i.e.* the reversible participation of the oxygen anion to the redox properties that occurs without major structural reorganisation, on the contrary to the irreversible loss of oxygen that would imply large cationic migration and densification of the host structure. By screening the particles of the (electrochemically or chemically) cycled materials from the surface to the bulk, we have shown that domains with defects are formed at the external part of the particle only, and that no structural modification is observed within the bulk. The defects are the results of transition metal ions migration from the transition metal layers to the Li layers. In addition to these defects, there is also a migration of the transition metal ions into the vacancies formed in the transition metal layers by Li deintercalation during the first charge at high voltage. This latter observation fully supports the occurrence of a densification process at the external part of the particles, implying

irreversible oxygen loss and migration of transition metal from the outer surface to the "bulk". In previous studies (electrochemical characterization[24] and neutron diffraction of the material recovered after one chemical cycle[25]) we have shown that during the plateau ca. 0.40 electrons are extracted to oxidize oxygen within the material (bulk) and ca. 0.30 to oxidize oxygen on the surface (with oxygen evolution and densification). These results are in rather good agreement with the observations reported here.

The essential information obtained from these high resolution microscopy and nano-diffraction experiments is that no significant structural modifications occur within the bulk of the particles during the first cycle and thus that the "plateau" is not mainly associated to oxygen loss, again supporting the reversible oxidation of oxygen ions (without oxygen loss) in the core of particles.

ACKNOWLEDGEMENTS

The authors thank CNRS, Région Aquitaine and Toyota Motor Europe for financial support.

SUPPORTING INFORMATION AVAILABLE

Additional table: Table S1 gives the description of the cationic distribution in the transition metal layers, by analogy with Li_2MnO_3 in the C2/m space group. This information is available free of charge via the Internet at http://pubs.acs.org.

REFERENCES

(1) Thackeray, M.M.; Wolverton, C.; Isaacs, E.D. Electrical Energy Storage for Transportation-Approaching the Limits of, and Going Beyond, Lithium-ion Batteries. *Energy Environ. Sci.*, **2012**, *5*, 7854-7863.

(2) Kim, Y.J.; Jung, H.G.; Scrosati, B.; Sun, Y.K. Synthesis of $Li[Li_{1.19}Ni_{0.16}Co_{0.08}Mn_{0.57}]O_2$ Cathode Materials with a High Volumetric Capacity for Li-ion Batteries. *J. Power Sources*, **2012**, *203*, 115-120.

(3) Croy, J.R.; Gallagher, K.G.; Balasubramanian, M.; Long, B.R.; Thackeray, M.M. Quantifying Hysteresis and Voltage Fade in $xLi_2MnO_3\bullet(1-x)LiMn_{0.5}Ni_{0.5}O_2$ Electrodes as a Function of Li_2MnO_3 Content. *J. Electrochem. Soc.* **2014**, *161*, A318-A325.

(4) Lee, J.; Urban, A.; Li, X.; Su, D.; Hautier, G. ; Ceder, G. Unlocking the Potential of Cation-Disordered Oxides for Rechargeable Lithium Batteries. *Science* **2014**, *343*, 519-522.

(5) Ohzuku, T.; Nagayama, M.; Tsuji, K.; Ariyoshi, K. High-capacity Lithium Insertion Materials of Lithium Nickel Manganese Oxides for Advanced Lithium-ion Batteries: toward Rechargeable Capacity more than 300 mAh.g-1. *J. Mater. Chem.* **2011**, *21*, 10179-10188.

(6) Thackeray, M. M.; Johnson, C. S.; Vaughey, J. T.; Li, N.; Hackney, S. A. Advances in Manganese-Oxide 'Composite' Electrodes for Lithium-ion Batteries. *J. Mater. Chem.* **2005**, *15*, 2257-2267.

(7) Thackeray, M. M.; Kang, S.-H.; Johnson, C. S.; Vaughey, J. T.; Hackney, S. A. Comments on the Structural Complexity of Lithium-rich $Li_{1+x}M_{1-x}O_2$ Electrodes (M = Mn, Ni, Co) for Lithium Batteries. *Electrochem. Commun.* **2006**, *8*, 1531-1538.

(8) Thackeray, M. M.; Kang, S.-H.; Johnson, C. S.; Vaughey, J. T.; Benedek, R.; Hackney, S. A. Li_2MnO_3-stabilized $LiMO_2$ (M = Mn, Ni, Co) Electrodes for Lithium-ion Batteries. *J. Mater. Chem.* **2007**, *17*, 3112-3125.

(9) Yu, H.; Ishikawa, R.; So, Y.-G.; Shibata, N.; Kudo, T.; Zhou, H.; Ikuhara, Y. Direct Atomic-Resolution Observation of Two Phases in the $Li_{1.2}Mn_{0.567}Ni_{0.166}Co_{0.067}O_2$ Cathode Material for Lithium-Ion Batteries. *Angew. Chem. Int. Ed*. **2013**, *52*, 5969-5973.

(10) Lu, Z.; Chen, Z.; Dahn, J. R. Lack of Cation Clustering in $Li[Ni_xLi_{1/3-2x/3}Mn_{2/3-x/3}]O_2$ ($0 < x \leq 1/2$) and $Li[Cr_xLi_{(1-x)/3}Mn_{(2-2x)/3}]O_2$ ($0 < x < 1$). *Chem. Mater.* **2003**, *15*, 3214-3220.

(11) Lei, C.H.; Bareno, J.; Wen, J.G.; Petrov, I.; Kang, S.-H.; Abraham, D.P. Local Structure and Composition Studies of $Li_{1.2}Ni_{0.2}Mn_{0.6}O_2$ by Analytical Electron Microscopy. *J. Power Sources* **2008**, *178*, 422-433.

(12) Jarvis, K. A.; Deng, Z.; Allard, L. F.; Manthiram, A.; Ferreira, P. J. Atomic Structure of a Lithium-Rich Layered Oxide Material for Lithium-Ion Batteries: Evidence of a Solid Solution. *Chem. Mater.* **2011**, *23*, 3614-3621.

(13) Wen, J.G.; Bareno, J.; Lei, C.H.; Kang, S.H.; Balasubramanian, M.; Petrov, I.; Abraham, D.P. Analytical Electron Microscopy of $Li_{1.2}Co_{0.4}Mn_{0.4}O_2$ for Lithium-ion Batteries. *Solid State Ionics* **2011**, *182*, 98-107.

(14) Bareno, J.; Balasubramanian, M.; Kang, S. H.; Wen, J. G.; Lei, C. H.; Pol, S. V.; Petrov, I.; Abraham, D. P. Long-Range and Local Structure in the Layered Oxide $Li_{1.2}Co_{0.4}Mn_{0.4}O_2$. *Chem. Mater.* **2011**, *23*, 2039-2050.

(15) Koga, H.; Croguennec, L.; Mannessiez, Ph.; Ménétrier, M.; Weill, F.; Bourgeois, L.; Duttine, M.; Suard, E.; Delmas, C. $Li_{1.20}Mn_{0.54}Co_{0.13}Ni_{0.13}O_2$ with Different Particle Sizes as Attractive Positive Electrode Materials for Lithium-Ion Batteries: Insights into Their Structure. *J. Phys. Chem. C* **2012**, *116*, 13497−13506.

(16) McCalla, E.; Rowe, A. W.; Shunmugasundaram, R.; Dahn, J. R. Structural Study of the Li−Mn−Ni Oxide Pseudoternary System of Interest for Positive Electrodes of Li-Ion Batteries. *Chem. Mater.*, **2013**, *25*, 989-999.

(17) McCalla, E.; Lowartz, C. M.; Brown, C. R.; Dahn, J. R. Formation of Layered–Layered Composites in the Li–Co–Mn Oxide Pseudoternary System during Slow Cooling. *Chem. Mater.*, **2013**, *25*, 912-918.

(18) McCalla, E.; Rowe, A. W.; Brown, C. R.; Hacquebard, P.; Dahn, J. R., How Phase Transformations during Cooling Affect Li-Mn-Ni-O Positive Electrodes in Lithium Ion Batteries. *J. Electrochem. Soc.*, **2013**, *160*, A1134-A1138.

(19) McCalla, E.; Li, J.; Rowe, A. W. ; Dahn, J. R., The Negative Impact of Layered-Layered Composites on the Electrochemistry of Li-Mn-Ni-O Positive Electrodes for Lithium-Ion Batteries. *J. Electrochem. Soc.*, **2014**, *161*, A606-A613.

(20) Boulineau, A.; Croguennec, L.; Delmas, C.; Weill, F. Structure of Li2MnO3 with Different Degrees of Defects. *Solid State Ionics* **2010**, *180*, 1652-1659.

(21) Boulineau, A.; Croguennec, L.; Delmas, C.; Weill, F. Reinvestigation of Li2MnO3 Structure: Electron Diffraction and High Resolution TEM. *Chem. Mater*., **2009**, *21*, 4216-4222.

(22) Weill, F.; Tran, N.; Croguennec, L.; Delmas, C. Cation Ordering in the Layered $Li_{1+x}(Ni_{0.425}Mn_{0.425}Co_{0.15})_{1-x}O_2$ Materials (x = 0 and 0.12). *J. Power Sources* **2007**, *172*, 893-900.

(23) Howie A. Image Contrast and Localized Signal Selection Techniques. *J. Microscopy*, **1979**, *117*, 11-23.

(24) Koga, H.; Croguennec, L.; Ménétrier, M. ; Mannessiez, P.; Weill, F.; Delmas, C. Different Oxygen Redox Participation for Bulk and Surface: A Possible Global Explanation for the Cycling Mechanism of $Li_{1.20}Mn_{0.54}Co_{0.13}Ni_{0.13}O_2$. *J. Power Sources,* **2013**, *236*, 250−258.

(25) Koga, H.; Croguennec, L.; Ménétrier, M.; Douhil, K.; Belin, S.; Bourgeois, L.; Suard, E.; Weill, F.; Delmas, C. Reversible Oxygen Participation to the Redox Processes Revealed for $Li_{1.20}Mn_{0.54}Co_{0.13}Ni_{0.13}O_2$. *J. Electrochem. Soc.* **2013**, *160*, A786−A792.

(26) Koga, H.; Croguennec, L.; Ménétrier, M.; Mannessiez, P.; Weill, F.; Delmas, C.; Belin, S. Operando X-ray Absorption Study of the Redox Processes Involved upon Cycling of the Li-Rich Layered Oxide $Li_{1.20}Mn_{0.54}Co_{0.13}Ni_{0.13}O_2$ in Li Ion Batteries. *J. Phys. Chem. C* **2014**, *118*, 5700–5709.

(27) Sathiya, M. ; Rousse, G. ; Ramesha, K. ; Laisa, C. P. ; Vezin, H. ; Sougrati, M. L. ; Doublet, M. L. ; Foix, D. ; Gonbeau, D. ; Walker, W. et al. Reversible Anionic Redox Chemistry in High-Capacity Layered-Oxide Electrodes. *Nat. Mater.* **2013**, *12*, 827-835.

(28) Boulineau, A.; Simonin, L.; Colin, J.- F.; Canevet, E.; Daniel, L.; Patoux, S. Evolutions of $Li_{1.2}Mn_{0.61}Ni_{0.18}Mg_{0.01}O_2$ during the Initial Charge/Discharge Cycle Studied by Advanced Electron Microscopy. *Chem. Mater.*, **2012**, *24*, 3558-3566

(29) Ito, A.; Shoda, K.; Sato, Y.; Hatano, M.; Horie, H.; Ohsawa, Y. Direct Observation of the Partial Formation of a Framework Structure for Li-rich Layered Cathode Material $Li[Ni_{0.17}Li_{0.2}Co_{0.07}Mn_{0.56}]O_2$ upon the First Charge and Discharge. *J. Power. Sources*, **2011**, *196*, 4785-4790.

(30) Reed, J.; Ceder, G.; Van der Ven, A. Layered-to-Spinel Phase Transition in Li_xMnO_2 *Electrochem. Solid State Lett.*, **2001**, *4*, A78-A81.

(31) Boulineau, A.; Simonin, L.; Colin, J.F.; Bourbon, C.; Patoux, S. First Evidence of Manganese−Nickel Segregation and Densification upon Cycling in Li-Rich Layered Oxides for Lithium Batteries. *Nano Lett.*, **2013**, *13*, 3857-3863.

(32) Capitaine, F.; Gravereau, P.; Delmas, C. A New Variety of $LiMnO_2$ with a Layered Structure. *Solid State Ionics* , **1996**, *89*, 197-202.

(33) Armstrong, A.R.; Bruce, P.G. Synthesis of Layered $LiMnO_2$ as an Electrode for Rechargeable Lithium Batteries. *Nature,* **1996**, *381*, 499-500.

(34) Sathiya, M.; Ramesha, K.; Rousse, G. ; Foix, D. ; Gonbeau, D. ; Prakash, A. S. ; Doublet, M. L. ; Hemalatha, K. ; Tarascon, J.-M. High Performance $Li_2Ru_{1-y}Mn_yO_3$ ($0.2 \leq y \leq 0.8$) Cathode Materials for Rechargeable Lithium-Ion Batteries: Their Understanding. *Chem Mater,* **2013**, *25*, 1121-1131.

(35) Sathiya, M. ; Abakumov, A. M.; Foix, D. ; Rousse, G. ; Ramesha, K.; Saubanère, M.; Doublet, M. L.; Vezin, H. ; Laisa, C. P. ; Prakash, A. S. et al. Origin of Voltage Decay in High-capacity Layered Oxide Electrodes, *Nat. Mater.* DOI:10.1038/NMAT4137

FIGURE CAPTIONS

Figure 1: Representation of the transition metal ordering in the slab for the Li_2MnO_3 composition. The blue line indicates the basic plane of the classical cell for layered structure (R-3m); the red dotted line indicates the basic plane of the superstructure cell and the arrows indicate the projection directions used in the HAADF STEM study in the following of the paper.

Figure 2: Charge and discharge curves typical of Li//$Li_{1.20}Mn_{0.54}Co_{0.13}Ni_{0.13}O_2$ cells, depending on the potential window. The studied materials, recovered from batteries, are highlighted by black points.

Figure 3: Experimental HAADF STEM image of $Li_{1.20}Mn_{0.54}Co_{0.13}Ni_{0.13}O_2$. The solid red, blue and green lines underline the different stacking of the slabs. The red arrows indicate partially apparently non ordered transition metal layers. In inset is given for comparison an image simulated considering the successive stacking along the $c_{hex.}$ axis of two ordered domains twinned of 60°.

Figure 4: Projection of the Li_2MnO_3 structure along the three directions indicated by arrows in figure 1: (a) along $[120]_{R\text{-}3m}$, (b) along $[210]_{R\text{-}3m}$ and (c) along $[\text{-}110]_{R\text{-}3m}$. The corresponding diffraction patterns are also shown. Indexations correspond to the R-3m space group and the red arrows indicate the lines with reflections due to the ordering of the transition metal in the layers.

Figure 5: Comparison of the experimental (a) and simulated (b) electron diffraction patterns of $Li_{1.20}Mn_{0.54}Co_{0.13}Ni_{0.13}O_2$. The simulation was performed considering Li_2MnO_3 with the cell parameters of $Li_{1.20}Mn_{0.54}Co_{0.13}Ni_{0.13}O_2$ and the stacking of 3 slabs-containing domains showing two different orientations.

Figure 6: Typical electron nano-diffraction patterns obtained for one crystallite of $Li_{1.20}Mn_{0.54}Co_{0.13}Ni_{0.13}O_2$ (a): pattern observed in the area ⑥ of the crystal (b), pattern observed in the areas ④, ⑤, ⑧ and ⑨ (c) and pattern observed in the areas ①, ②, ③ and ⑦ (d). The red and blue lines underline the characteristic features of the patterns and are related to the lines of the same color displayed on the theoretical patterns given in figure 4.

Figure 7: Schematic representation of a domain wall in a crystal leading to the formation of an apparent non ordered layer (here made of blue dots (i.e. of transition metal ions M) only).

Figure 8: (a-b) Representative HAADF-STEM images of the material recovered after the 1st cycle of the battery without the “plateau”, at different scales and in different places in a particle. These images are representative of the bulk and of the outer part of the particles. (c-d)The corresponding images obtained for the material recovered after the 1st cycle of the battery with the “plateau”. White arrows indicate the

presence of transition metal ions into the Li layers. These images are representative of the outer part of the particles only; within the bulk the images obtained are similar to (a-b).

Figure 9: Representatives HAADF-STEM images of the material obtained after chemical Li reinsertion in a material previously chemically deintercalated, in the bulk (a) and at the surface (b) of a particle. In inset of (b) is given for comparison an image simulated considering the formation of pure spinel-type domain.

Figure 10: Zones of the crystal analyzed by nano-diffraction and the corresponding nano-diffraction patterns obtained for the material prepared chemically from $Li_{1.20}Mn_{0.54}Co_{0.13}Ni_{0.13}O_2$. The additional spots present between the diffusion lines reveal the formation of defects near the surface.

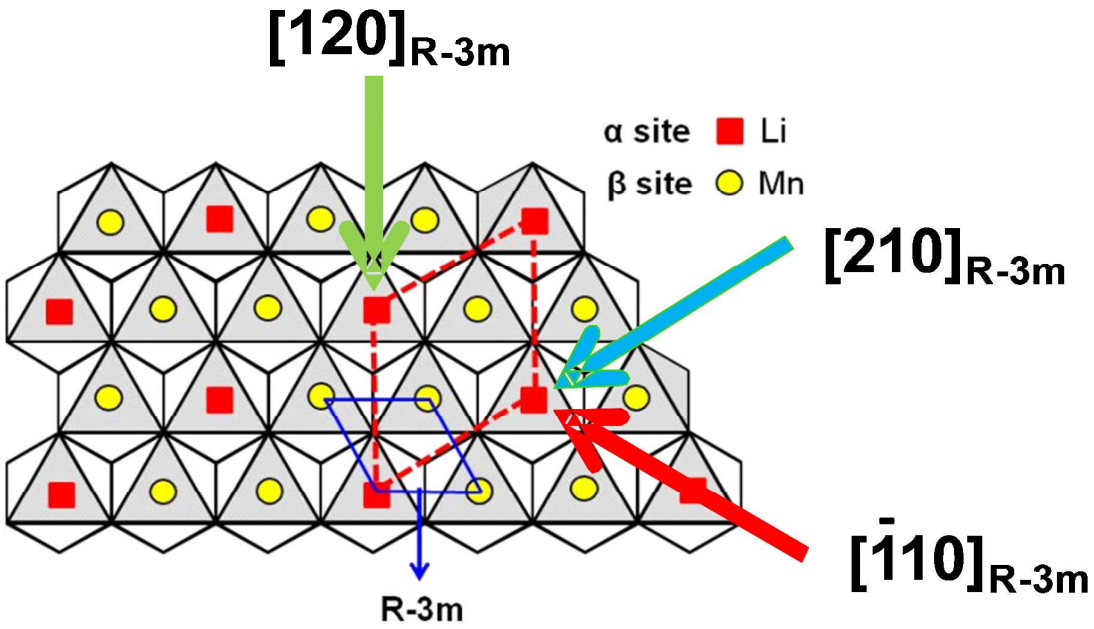

Figure 1: Representation of the transition metal ordering in the slab for the Li_2MnO_3 composition. The blue line indicates the basic plane of the classical cell for layered structure (R-3m); the red dotted line indicates the basic plane of the superstructure cell and the arrows indicate the projection directions used in the HAADF STEM study in the following of the paper.

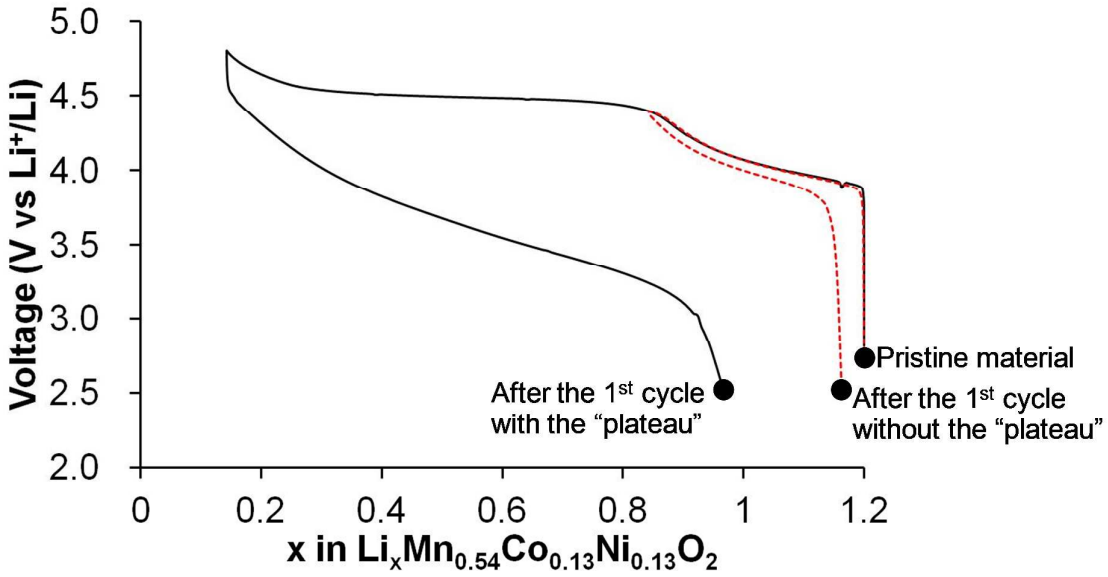

Figure 2: Charge and discharge curves typical of Li//$Li_{1.20}Mn_{0.54}Co_{0.13}Ni_{0.13}O_2$ cells, depending on the potential window. The studied materials, recovered from batteries, are highlighted by black points.

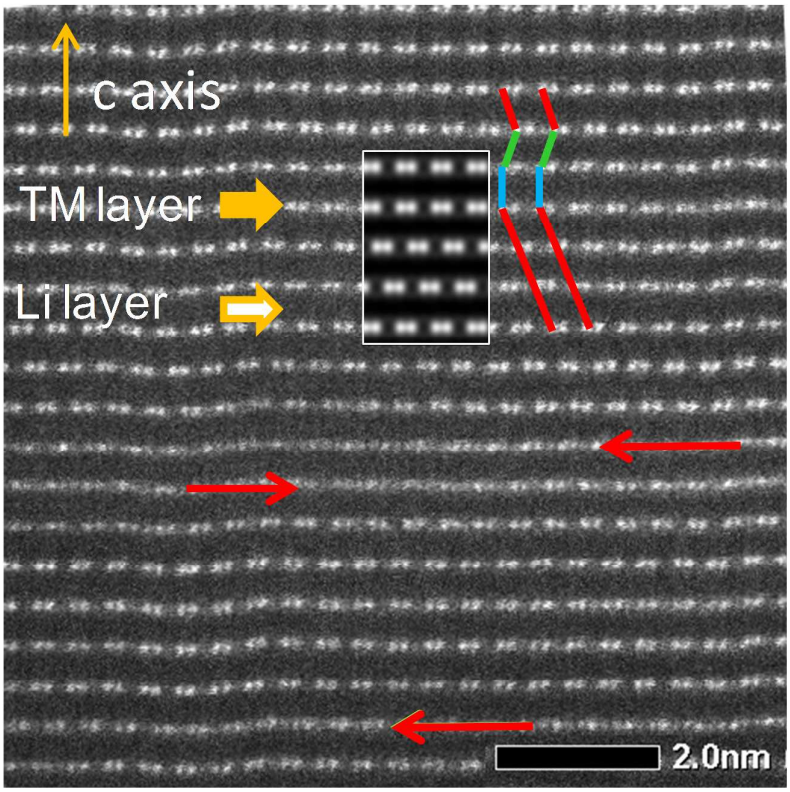

Figure 3: Experimental HAADF STEM image of $Li_{1.20}Mn_{0.54}Co_{0.13}Ni_{0.13}O_2$. The solid red, blue and green lines underline the different stacking of the slabs. The red arrows indicate partially apparently non ordered transition metal layers. In inset is given for comparison an image simulated considering the successive stacking along the $c_{hex.}$ axis of two ordered domains twinned of 60°.

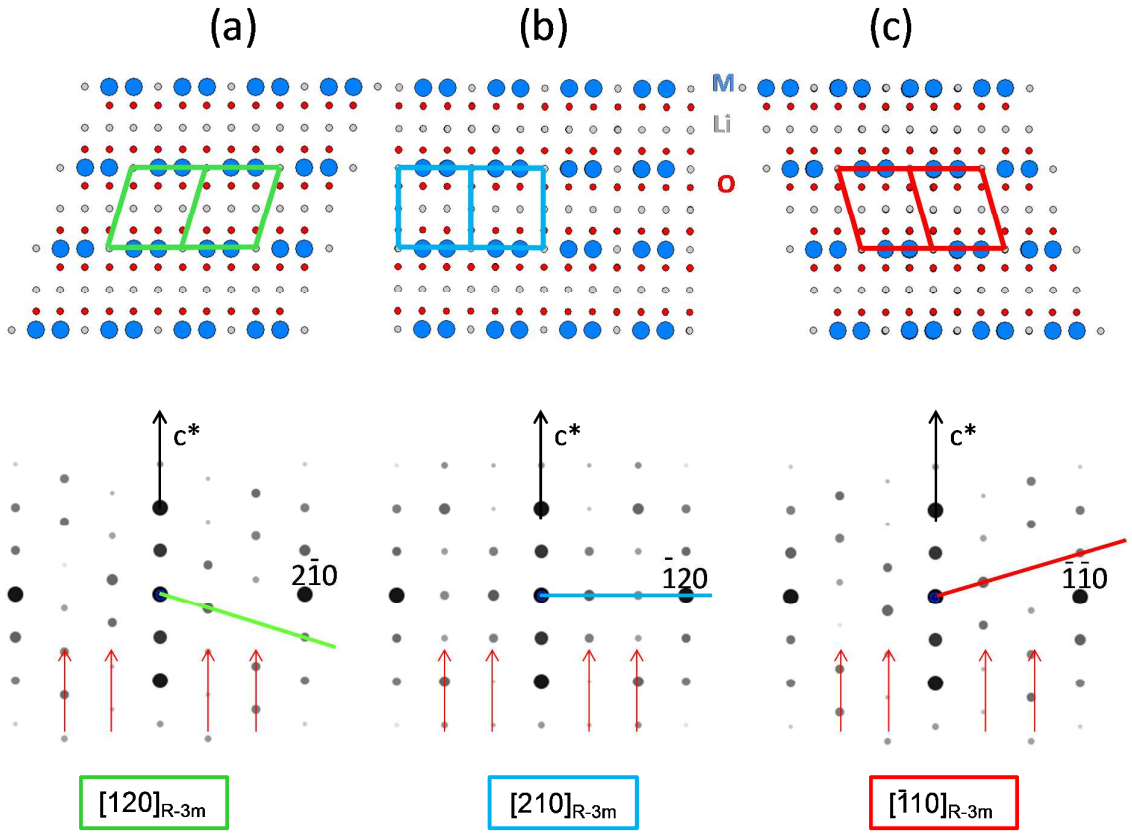

Figure 4: Projection of the Li_2MnO_3 structure along the three directions indicated by arrows in figure 1: (a) along $[120]_{R\text{-}3m}$, (b) along $[210]_{R\text{-}3m}$ and (c) along $[\text{-}110]_{R\text{-}3m}$. The corresponding diffraction patterns are also shown. Indexations correspond to the R-3m space group and the red arrows indicate the lines with reflections due to the ordering of the transition metal in the layers.

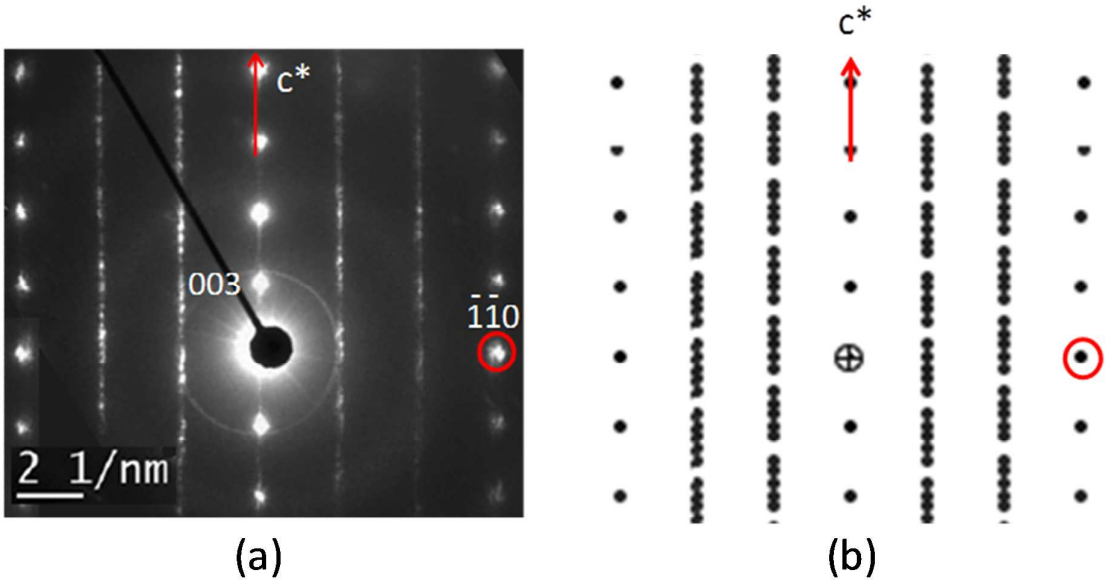

Figure 5: Comparison of the experimental (a) and simulated (b) electron diffraction patterns of $Li_{1.20}Mn_{0.54}Co_{0.13}Ni_{0.13}O_2$. The simulation was performed considering Li_2MnO_3 with the cell parameters of $Li_{1.20}Mn_{0.54}Co_{0.13}Ni_{0.13}O_2$ and the stacking of 3 slabs-containing domains showing two different orientations.

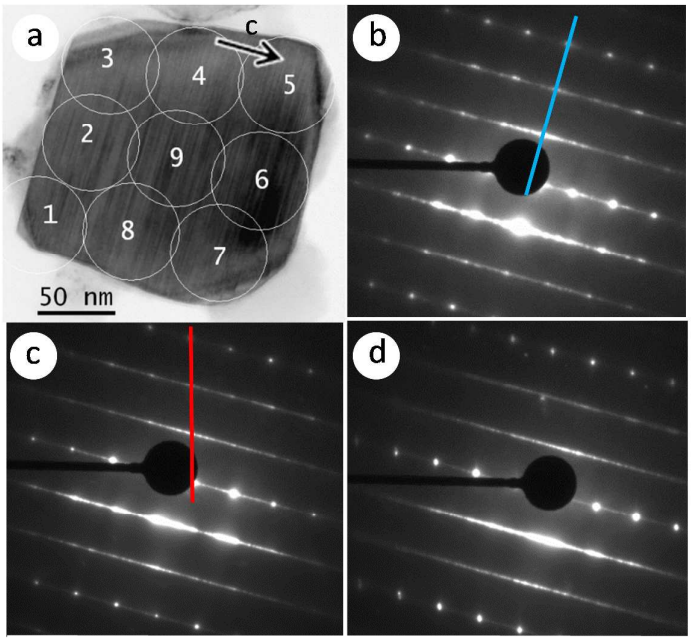

Figure 6: Typical electron nano-diffraction patterns obtained for one crystallite of $Li_{1.20}Mn_{0.54}Co_{0.13}Ni_{0.13}O_2$ *(a): pattern observed in the area ⑥ of the crystal (b), pattern observed in the areas ④, ⑤, ⑧ and ⑨ (c) and pattern observed in the areas ①, ②, ③ and ⑦ (d). The red and blue lines underline the characteristic features of the patterns and are related to the lines of the same color displayed on the theoretical patterns given in figure 4.*

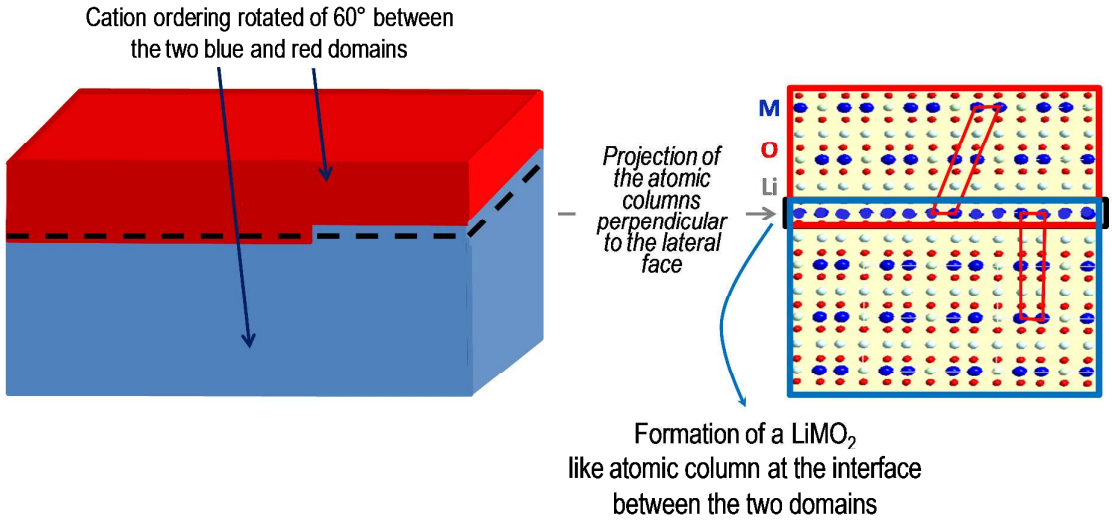

Figure 7: Schematic representation of a domain wall in a crystal leading to the formation of an apparent non ordered layer (here made of blue dots (i.e. of transition metal ions M) only).

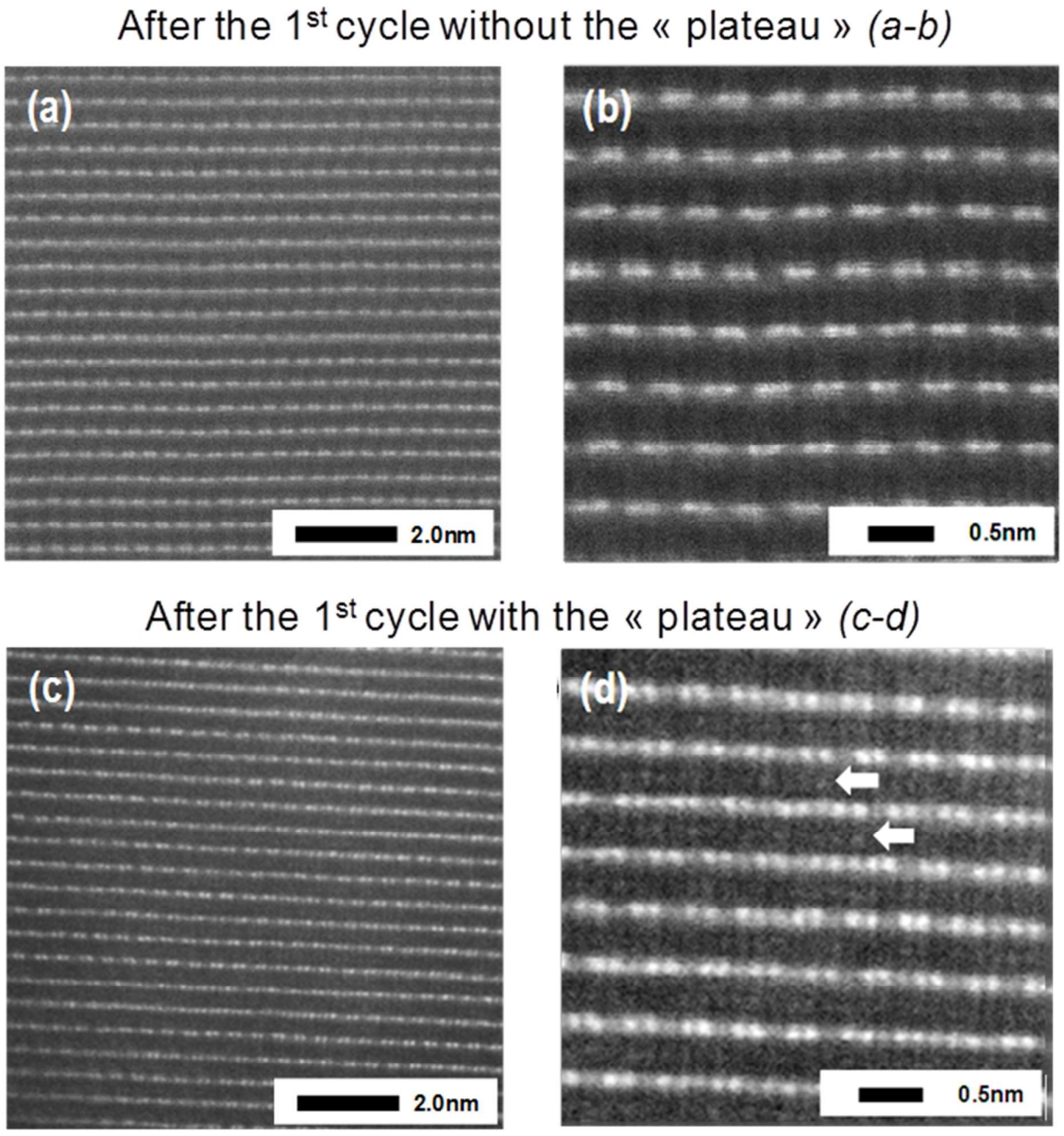

Figure 8: (a-b) Representative HAADF-STEM images of the material recovered after the 1st cycle of the battery without the "plateau", at different scales and in different places in a particle. These images are representative of the bulk and of the outer part of the particles. (c-d)The corresponding images obtained for the material recovered after the 1st cycle of the battery with the "plateau". White arrows indicate the presence of transition metal ions into the Li layers. These images are representative of the outer part of the particles only, within the bulk the images obtained are similar to (a-b).

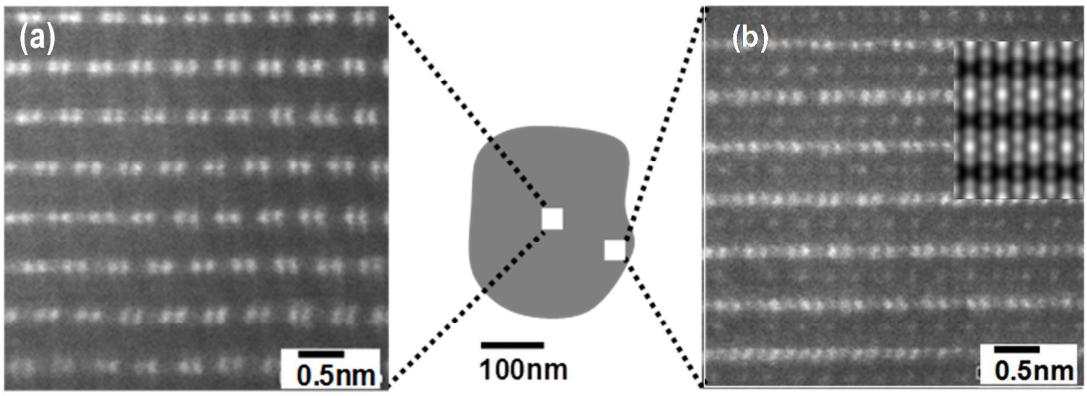

Figure 9: Representatives HAADF-STEM images of the material obtained after chemical Li reinsertion in a material previously chemically deintercalated, in the bulk (a) and at the surface (b) of a particle. In inset of (b) is given for comparison an image simulated considering the formation of pure spinel-type domain.

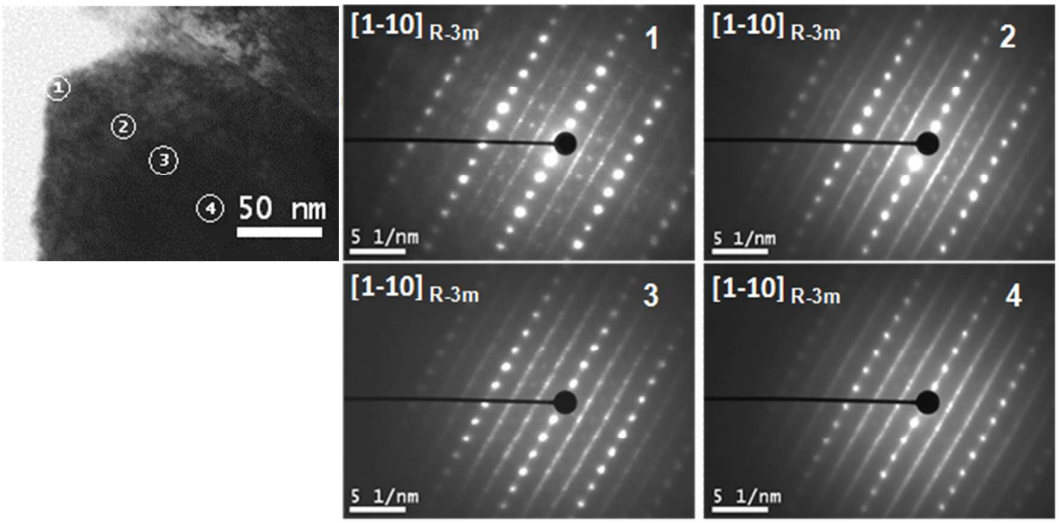

Figure 10: Zones of the crystal analyzed by nano-diffraction and the corresponding nano-diffraction patterns obtained for the material prepared chemically from $Li_{1.20}Mn_{0.54}Co_{0.13}Ni_{0.13}O_2$. The additional spots present between the diffusion lines reveal the formation of defects near the surface.

TABLE OF CONTENTS

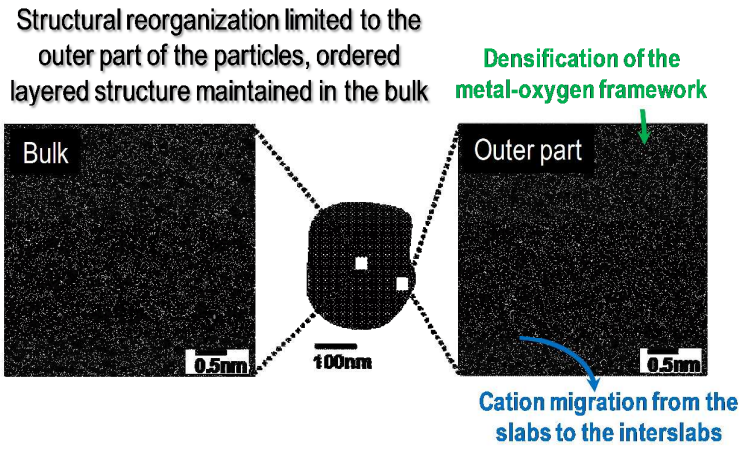

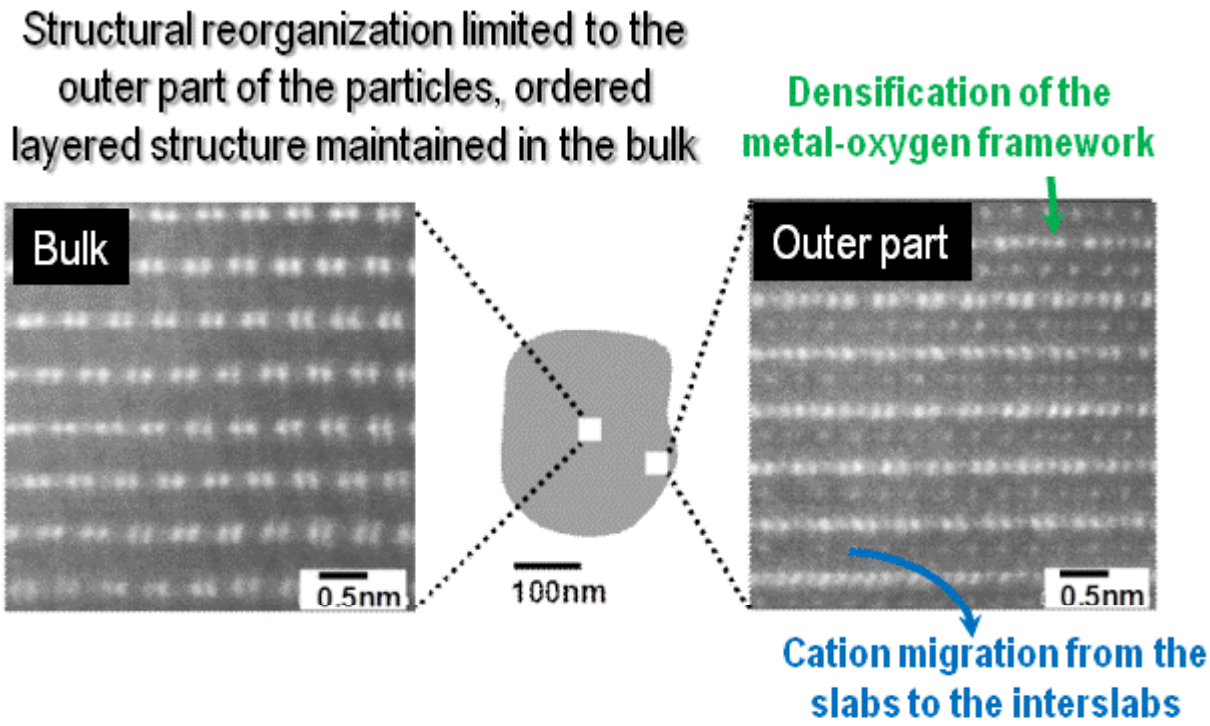
Structural reorganization limited to the outer part of the particles, ordered layered structure maintained in the bulk
Densification of the metal-oxygen framework
Bulk
Outer part
0.5nm
100nm
0.5nm
Cation migration from the slabs to the interslabs